Fundamental parameters for a minimal mass design of prismatic tensegrity cylinder subjected to a compressive force

Angelo Vumiliya, Ani Luo and Heping Liu
College of Mechanical and Electrical Engineering, Harbin Engineering University, Harbin, China, and
Andrés González
School of Mechanical Engineering, University of Costa Rica, San Pedro, Costa Rica

Received 26 May 2020
Revised 5 August 2020
13 September 2020
20 September 2020
Accepted 11 October 2020

Abstract

Purpose – This paper aims to propose a study on the static behavior of prismatic tensegrity structures and an innovative form for determining the effect of mechanical properties and geometric parameters on the minimal mass design of these structures.

Design/methodology/approach – The minimal mass design in this paper considers a stable class-two tensegrity tower built through stable models. Using the proposed structures, comprehensive parametric studies are performed to examine the mass (in which the masses of joints are ignored), the mass ratio between a class-two tensegrity tower and a single element, both having the same diameter and length and afterward determine a reliable mass saving structure under various circumstances.

Findings – The simulations show that the mass ratio versus the number of units is a nonlinear regressive curve and predicts that the proposed model outperforms the standard model when the variation parameter considered is a vertical force. The difference in mass between these structures is visible when the gap gradually decreases while the number of units increases. On the geometrical aspect, the gap between the masses is not significant.

Originality/value – This paper helps to understand the influences of geometric parameters and the mechanical properties on the design of cylinder tensegrity structures dealing with a compressive force.

Keywords Configuration, Typology, Equilibrium formulation, Mass ratio, Structural comparison

Paper type Research paper

1. Introduction

A tensegrity structure is a system in a self-stable state comprising a set of compressed components inside of tensioned components (René Motro, 2003). More precisely, the cables and bars serve for the tension and compression forces, respectively. The connection of these components focuses on a specific network of strength resistant to small disturbances (it is the perturbation occurred when the applied force vanishes) and making the design of stable structures more relevant. Indeed, the design may consist of: assessing the stability under external forces to minimize the mass by adjusting the shape and topology to prevent the materials from buckling (Goyal *et al.*, 2020); finding the feasible prestress through multi

The authors gratefully acknowledge the contribution of National Natural Science Fund of China (Grant Number 51875111) and National Science Fund of Heilongjiang Province (Grant Number LH2019E023).

Engineering Computations

0264-4401
DOI 10.1108/EC-05-2020-0284

self-stress states of predefined geometry (Chen *et al.*, 2018, 2020); and setting admissible forces through the positions of nodes, known as configuration, and a specific system connecting cables to struts in such a way that further similar configurations provide self-balanced structures.

For instance, the prismatic tensegrity has been studied extensively for its most straightforward principle of connecting the polygons located into two different planes. Figure 1 illustrates an example of self-stable tensegrities with the same number of bars but built with a different system of cables. The triangular prism system merges into a star tensegrity system by connecting the horizontal cables to the center (Zhang *et al.*, 2010); this requires extra nodes γ overlapping the top and the bottom center of the cylinder [Figure 1(a)]. The values of $\gamma \neq 0$ entail an increase in the number of cables or bars depending on the state of stress, respectively [Figure 1(b)]. Also, the algorithm proposed in Vumiliya *et al.* (2018) creates a stable system in which, without any adjustment, the structure obtained gives an illustration of a half-star in Figure 1(c). However, to maintain the rigidity of the new three-bars tensegrity proposed in Liu *et al.* (2018), the number of nodes and cables was increased in the configuration of a triangular model as in Figure 1(c).

Taking into consideration the properties of the different ways to connect cables to struts, one can design a structure with a specific response for predefined conditions. Therefore, this work proposes a new form of prismatic tensegrity characterized by an increase in the nodes on horizontal cables. The extra nodes lead to omit the vertical cables and replace them with additional cables. The proposed structure, inspired by the prismatic system, gives numerous advantages such as geometric symmetry, ease of construction, deformability and reduced volume. To determine further advantages, the proposed and standard models are compared through the design of a mass-saving structure under a compressive force. Various parameters affecting the performance are investigated in-depth; in this process, the large-scale tensegrities are obtained by the assembly of unitary models.

The outline of the paper is divided into six sections, as follows: Section 2 reviews the literature of recent work on prismatic tensegrities and illustrates used approaches to generate a structure with minimal mass. Section 3 presents the single pattern of the new structure obtained through the configuration of a single layer and classifies the components

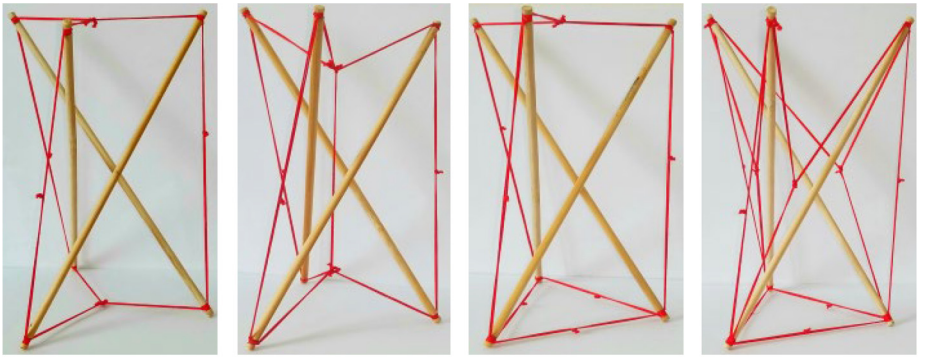

Notes: (a) Three struts tensegrity star; (b) three struts tensegrity star with an additional cable in spired by a model with an extra bar; (c) half-star three struts tensegrity; (d) a new three bars tensegrity unit

Figure 1.
Varieties of self-equilibrated three-struts tensegrity systems

into different categories. Section 4 gives the analytical formulation for the equilibrium where the expressions of self-stress are established by finding the force densities in members in terms of existing configuration and topology. Follows the use of the results in Section 4 for determining the mass of the above structures under a compressive force in Section 5. Section 6 gives a structural behavior comparison conducted through the mass ratio and the coefficient of reduction/amplification of mass. Finally, Section 7 briefly concludes the study of these cylinder models.

2. Survey of prismatic tensegrities

The term *prismatic* tensegrity stands on the fact that the structure has regular polygons located on parallel planes. Inspired by their regularity, various types of multi-unit tensegrities have originated from connecting prismatic cells and some assembly strategies can be found in Fazli and Abedian (2011), Liu *et al.* (2017); Xu and Luo (2010). However, their practical uses might lead to modifications of the prisms to achieve a given purpose (Caluwaerts *et al.*, 2016; Iscen *et al.*, 2013; Kim *et al.*, 2020). It is distinguished in Kawaguchi and Lu (2002) a pair of cones of a three-strut tension system constructed to support the structures for a membrane roof. Similarly, a tensegrity dome for humanitarian aid was built using three conic units (González *et al.*, 2017). Furthermore, the six-bar robot system *SUPERball*, used as a space exploration structure, combines two three-bar units with different radius (Agogino *et al.*, 2013). The above research studies have the common aspect of finding the relative stress of self-balanced structures. Consequently, multiple static and dynamic approaches were deployed for both regular and irregular tensegrities (Koohestani, 2017; Sultan *et al.*, 2002; Zhang *et al.*, 2018). See Tibert and Pellegrino (2003) and Zolesi *et al.* (2013) for an extensive review of these aspects.

However, the applications in structural engineering show the search for light structures, and new forms have become more relevant in recent decades (Averseng and Dubé, 2012; Fraddosio *et al.*, 2019; Ma *et al.*, 2019). For this, different approaches and experiments were conducted in the response of modeling the material and strategic assembly of different materials (Amendola *et al.*, 2014; Goyal *et al.*, 2020). Such studies show the comprehensive behavior in transfer from stiffening to softening under a large displacement influenced by geometry and prestress. In addition to this, a dynamic study performed based on masses establishes the feasible limit on the formation and propagation of the solitary wave (Fraternali *et al.*, 2012). Also, in Chen and Skelton (2020) a general approach is presented for the design of minimal mass of tensegrities using solid and hollow bars while ensuring the equilibrium condition. Skelton and De Oliveira (2010) focus on the concept of tensegrities as lightweight structures; they suggest using iterations of self-similar structures from the perspective of achieving a minimal mass with invariant compressive strength. It implies using the complexity of T-Bar and D-bar, where the system proposed reduces the mass compared to a single bar of the same length. Similarly, these structures are also proposed as mass-efficient energy absorption systems by reducing the impact in planetary landing (Goyal *et al.*, 2019) and further designed to improve their application as support of compressive forces in Goyal *et al.* (2020), Skelton *et al.* (2016). Besides this, the tensegrity towers and plates were also the subjects of study, where they are used as the physical mass saving structure according to the defined compressive force (De Oliveira *et al.*, 2008; Skelton and De Oliveira, 2010). These proposals treat the optimal complexity with a finite number of iterations under a vertical load. Despite the above results, still, some questions remain unanswered:

- Whether the self-similar prismatic unitary structure holds the character of mass saving structure given the number of layers at any magnitude of applied force.

- Whether the minimum mass can be parameterized considering the geometry (height and the radius of the cylinder).
- Whether it exists a structure that can outperform the prismatic tensegrity structure at the present applied force.

To this, the work proposed in this paper studies the static behavior of the prismatic tensegrity and the innovative tensegrity form for answering these unsolved questions.

3. Configuration and topology

Mainly four parameters contribute to the definition of nodal coordinates of the tensegrity structure: the radius r, the height h separating two planes, $\varphi = 2\pi/g$, the angle between two consecutive nodes located on the same horizontal plane, where g is the total number of bars and a twist angle α relating a rotation between the bottom and top prism. The nodal position of the k-th strut in Figure 2(b) and 2(c) is expressed by a tridimensional vector $\mathbf{b}_k$ given as:

$$\mathbf{b} = \begin{pmatrix} x_i \\ y_i \\ z_i \end{pmatrix} - \begin{pmatrix} x_j \\ y_j \\ z_j \end{pmatrix}; \quad \begin{cases} k = 1, 2, \ldots, g \\ i = j = k \end{cases} \tag{1}$$

in which $(x_i, y_i, z_i) = r(\cos\varphi, \sin\varphi, 0)$ is the bottom node and $(x_j, y_j, z_j) = r(\cos\theta, \sin\theta, h/r)$ is the top node rotated about the z-axis an angle $\theta = \varphi + \alpha$. However, r and h are variable while α is the main characteristic defining a self-stable prismatic tensegrity (Luo *et al.*, 2018) given as:

$$\alpha = \frac{\pi}{2} - \frac{\pi}{g} \tag{2}$$

Figure 2(b) represents a strut of a prismatic tensegrity, which serves as a connection framework for horizontal ($\mathbf{s}_h$) and vertical ($\mathbf{s}_v$) cables, while Figure 2(c) is the same configuration of the strut as in Figure 2(b) with additional nodes on the horizontal cables,

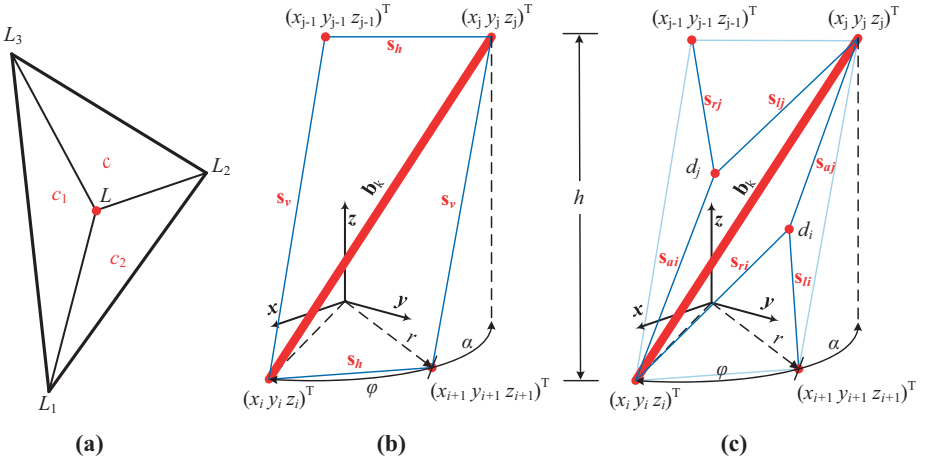

Figure 2.
Configuration of a tensegrity strut in the global coordinate systemNotes: (a) Barycentric coordinates; (b) prismatic tensegrity structure; and (c) novel tensegrity.

Notes: (a) Barycentric coordinates; (b) prismatic tensegrity structure; (c) novel tensegrity

resulting in additional cables ($\mathbf{s}_{ai}$, $\mathbf{s}_{aj}$) when the vertical cables are suppressed. The additional nodes divide the horizontal cables into two cables $\mathbf{s}_{rj}$ and $\mathbf{s}_{lj}$ on top and in $\mathbf{s}_{ri}$ and $\mathbf{s}_{li}$ on bottom, respectively. The additional bottom and top nodes on the horizontal cables are established through the barycentric coordinates. Figure 1(a) illustrates the example of the barycentric coordinates used to express the position of any point L located inside the triangle of vertices L_1, L_2 and L_3. The node L is computed using the following expression:

$$L = c_1 L_3 + c_2 L_2 + c L_1 \tag{3}$$

in which c_1, c_2 and c are real numbers such that c_1+c_2+c = 1. From this, the scalar c can be found as c = 1-c_1-c_2, which implies $c_1 + c_2 < 1$. Hence, by replacing the value of the scalar c in equation (3), the point L becomes:

$$L = c_1 L_3 + c_2 L_2 + (1 - c_1 - c_2) L_1 \tag{4}$$

Applying the same concept to the prismatic tensegrity, the additional nodes of the new tensegrity are given as:

$$\begin{aligned} &\{ d_j = c_1 \begin{pmatrix} x_{-1} & y_{-1} & z_{-1} \end{pmatrix} + c_2 (xyz) + (1 - c_1 - c_2) \begin{pmatrix} x_i & y_i & z_i \end{pmatrix} d_i = c_3 \begin{pmatrix} x_i & y_i & z_i \end{pmatrix} \\ &+ c_4 \begin{pmatrix} x_{i+1} & y_{i+1} & z_{i+1} \end{pmatrix} + (1 - c_3 - c_4)(xyz) \end{aligned} \tag{5}$$

The prismatic structure is attained by closing the patterns of nodes as follows: horizontal cables connect the bottom and top vertex on each plane. The vertical distance that connects the top and the bottom node of two different bars defines relative height h between two planes; therefore, $3g$ (with $g \geq 3$) is the maximum number of cables needed to build a prismatic tensegrity structure. However, with the removal of vertical cables, the prototype of the novel tensegrity structure requires additional cables. In this view, the novel structure requires in total of 6 g cables.

Table 1 gives the characterization of components and classifies them into different categories based on the connection and the element's location (for instance, a prismatic tensegrity has two regular polygons formed by horizontal cables on two parallel planes which are considered as one category of cables).

4. Equilibrium formulation

This section presents formulas for self-balanced tensegrities based on nodal location and force density of components. The purpose is to find the right prestress congruent with the configuration (Koohestani and Guest, 2013; Zhang *et al.*, 2018); consequently, one seeks to determine the self-stress satisfying the following equilibrium equation:

$$\mathbf{Q} \begin{bmatrix} \mathbf{e_x} & \mathbf{e_y} & \mathbf{e_z} \end{bmatrix} = 0 \tag{6}$$

in which $\mathbf{Q} \in \mathbb{R}^{n \times n}$ (n: number of nodes) is the force density matrix and $\mathbf{e_x}$, $\mathbf{e_y}$, and $\mathbf{e_z}$ represent column vectors of nodal locations in x- y- and z-direction, respectively. The force density matrix is expressed using the addition operation (Tran and Lee, 2010) where the

Starting node	$i+1$	i (j)	d_i (d_j)	d_i (d_j)	d_i (d_j)	i
End node	j	$i+1$ (j−1)	i (j−1)	$i+1$ (j)	j (i)	j
Vector notation	$\mathbf{s}_v$	$\mathbf{s}_h$	$\mathbf{s}_{ri}$ ($\mathbf{s}_{rj}$)	$\mathbf{s}_{li}$ ($\mathbf{s}_{lj}$)	$\mathbf{s}_{aj}$ ($\mathbf{s}_{ai}$)	$\mathbf{b}_k$
Appellation	vertical	horizontal	right cable	left cable	additional	strut

Table 1. Classification of components

elements $\mathbf{Q}(i,l)$ are the sum of force densities of all p components meeting at i such $l = i$ and becomes a negative force density of a component that connects l and i for $l \neq i$:

$$\mathbf{Q}_{(i,l)} = \begin{cases} \sum \delta_p & if\ i = l \\ -\delta_p & if\ i \neq l\ and\ p\ connects\ l\ and\ i \\ 0 & otherwise \end{cases} \tag{7}$$

The set of nodal coordinates found by solving equation (6) should respond to the prototype of the configuration set in Section 3. However, the homogeneous system of equation (6) requires a nontrivial solution to guarantee the singularity and semi-positive definitiveness of the force density matrix. For this, the rank is n-4 for a three-dimensional structure; the null space of the force density matrix has a dimension of four. It is one of the well-known super-stability conditions of a three-dimensional tensegrity.

4.1 Self-stress of unitary tensegrity structures

From the classification made in Table 1, the horizontal cable, vertical cable and strut of a prismatic tensegrity are assigned the force densities as δ_h, δ_v and δ_b, respectively. The strategy of finding stresses implemented using equation (6), where the variable l in $\mathbf{Q}_{(i,l)}$ considers only the p members connected to the node (x_i, y_i, z_i):

$$\begin{array}{c} l \\ i-1 \\ i \\ i+1 \\ j-1 \\ j \end{array} \quad \begin{array}{c} \mathbf{Q}_{(i,l)} \\ \begin{pmatrix} -\delta_h \\ 2\delta_h + \delta_v + \delta_b \\ -\delta_h \\ -\delta_v \\ -\delta_b \end{pmatrix}^T \end{array} \quad \begin{array}{c} \begin{bmatrix} \mathbf{e_x} & \mathbf{e_y} & \mathbf{e_z} \end{bmatrix} \\ \begin{pmatrix} x_{i-1} & y_{i-1} & z_{i-1} \\ x_i & y_i & z_i \\ x_{i+1} & y_{i+1} & z_{i+1} \\ x_{j-1} & y_{j-1} & z_{j-1} \\ x_j & y_j & z_j \end{pmatrix} \end{array} = 0 \tag{8}$$

gives the self-stress congruent with the geometry as:

$$\begin{pmatrix} \delta_h \\ \delta_v \end{pmatrix} = \begin{pmatrix} \dfrac{x_i(\delta_v + \delta_b) - \delta_b x - x_{j-1}\delta_v}{x_{i+1} - 2x_i + x_{i-1}} & \dfrac{z_j\delta_b + (z_{i+1} + z_{i-1})\delta_h + z_i(\delta_b + 2\delta_h)}{z_i + z_{j-1}} \end{pmatrix} \tag{9}$$

The value in equation (9) holds for the twist angle given in equation (2); otherwise, the structure may not return to its initial configuration after unloading the system. Concerning the new tensegrity, the consideration of a symmetrical configuration leads to an assumption of symmetrical equilibrium at each node numbered with the same subscript i and j. Consequently, the internal forces in cables are defined as δ_{ri} (δ_{rj}), δ_{li} (δ_{lj}) and δ_{ai} (δ_{aj}), compatible with Table 1. However, the sequence of members for closing the pattern in Figure 2(c) increases on the bottom and top elements, which leads to a trivial solution for solving the homogeneous equilibrium system of p members that connect l to a node $(x_i\, y_i\, z_i)$:

$$\begin{array}{c} l \\ i \\ j \\ d_{i-1} \\ d_i \\ d_j \end{array} \quad \begin{array}{c} \mathbf{Q}_{(i,l)} \\ \begin{pmatrix} \delta_{li} + \delta_{ri} + \delta_{ai} + \delta_b \\ -\delta_b \\ -\delta_{li} \\ -\delta_{ri} \\ -\delta_{ai} \end{pmatrix}^T \end{array} \quad \begin{array}{c} \begin{bmatrix} \mathbf{e_x} & \mathbf{e_y} & \mathbf{e_z} \end{bmatrix} \\ \begin{pmatrix} x_i & y_i & z_i \\ x_j & y_j & z_j \\ d_{xi-1} & d_{yi-1} & d_{zi-1} \\ d_{xi} & d_{yi} & d_{zi} \\ d_{xj} & d_{yj} & d_{zj} \end{pmatrix} \end{array} = 0 \tag{10}$$

Therefore, the additional nodes are rewritten in the local coordinates system (Figure 3) to overcome the trivial solution by reducing the number of unknowns.

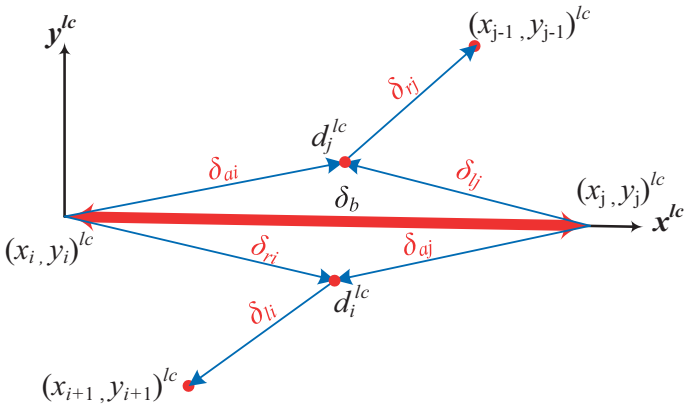

Note: The superscript *lc* represents the corresponding nodes in the local planar system

Figure 3.
Illustration of a pattern describing the local planar coordinate system of components connected on a strut

As in Liu *et al.* (2018), the nodes d_j^{lc} and d_i^{lc} are written as:

$$\begin{cases} d_{jx}^{lc} = c_1 x_j^{lc} + c_2 x_{j-1}^{lc} \\ d_{jy}^{lc} = c_2 y_{j-1}^{lc} \end{cases}, \quad x_i^{lc} = 0, \; y_i^{lc} = 0, \; y_j^{lc} = 0 \tag{11}$$

in which the subscript x and y represents the respective axis direction. The relationship between the force densities and the local nodal coordinates is obtained by using the equation representing the homogeneous linear system of equilibrium where on node d_j^{lc} is as:

$$\begin{cases} \left(x_{j-1}^{lc} - d_{jx}^{lc}\right)\delta_{rj} + \left(x_j^{lc} - d_{jx}^{lc}\right)\delta_{lj} - d_{jx}^{lc}\delta_{ai} = 0 \\ \left(y_{j-1}^{lc} - d_{jy}^{lc}\right)\delta_{rj} - d_{jy}^{lc}\delta_{lj} - d_{jy}^{lc}\delta_{ai} = 0 \end{cases} \tag{12}$$

Then, by substituting equation (11) into equation (12) and, after simplification, it is deduced:

$$\begin{cases} x_{j-1}^{lc}(\delta_{rj} - c_2\delta_{rj} - c_2\delta_{lj} - c_2\delta_{ai}) + x_j^{lc}(\delta_{lj} - c_1\delta_{lj} - c_1\delta_{rj} - c_1\delta_{ai}) = 0 \\ y_{j-1}^{lc}(\delta_{rj} - c_2\delta_{rj} - c_2\delta_{lj} - c_2\delta_{ai}) = 0 \end{cases} \tag{13}$$

Knowing the local nodal coordinates are non-null values, the relationship between force densities is:

$$\begin{pmatrix} \delta_{lj} \\ \delta_{rj} \end{pmatrix} = \begin{pmatrix} \dfrac{c_1\delta_{ai}}{1 - c_1 - c_2} \\ \dfrac{c_2\delta_{ai}}{1 - c_1 - c_2} \end{pmatrix} \tag{14}$$

Following the same algorithm, by considering node $(x_j, y_j)^{lc}$ as the origin, the expression for the forces density satisfying the equilibrium of node d_i^{lc} is:

$$\begin{pmatrix} \delta_{li} \\ \delta_{ri} \end{pmatrix} = \begin{pmatrix} \dfrac{c_3 \delta_{aj}}{1 - c_3 - c_4} \\ \dfrac{c_4 \delta_{aj}}{1 - c_3 - c_4} \end{pmatrix} \tag{15}$$

The above expressions result from the local nodal coordinates and help to reduce the unknowns where equation (10) can be rewritten as:

$$\begin{array}{c} l \\ i \\ j \\ d_{i-1} \\ d_i \\ d_j \end{array} \begin{array}{c} \mathbf{Q}_{(i,l)} \\ \begin{pmatrix} \frac{c_3+c_4}{1-c_3-c_4}\delta_{aj} + \delta_{ai} + \delta_b \\ -\delta_b \\ \frac{c_3\delta_{aj}}{c_3+c_4-1} \\ \frac{c_4\delta_{aj}}{c_3+c_4-1} \\ -\delta_{ai} \end{pmatrix}^T \end{array} \begin{array}{c} \begin{bmatrix} \mathbf{e_x} & \mathbf{e_y} & \mathbf{e_z} \end{bmatrix} \\ \begin{pmatrix} x_i & y_i & z_i \\ x_j & y_j & z_j \\ d_{xi-1} & d_{yi-1} & d_{zi-1} \\ d_{xi} & d_{yi} & d_{zi} \\ d_{xj} & d_{yj} & d_{zj} \end{pmatrix} \end{array} = 0 \tag{16}$$

and gives δ_b in the z-direction as:

$$\delta_b = -(c_1 + c_2)\delta_{ai} - (c_3 + c_4)\delta_{aj} \tag{17}$$

However, using the same algorithm at the node (x_j, y_j, z_j) in the z-direction, the same force density leads to:

$$\delta_b = -(c_3 + c_4)\delta_{aj} - (c_1 + c_2)\delta_{ai} \tag{18}$$

To keep the structure in a self-balanced condition based on the symmetric assumptions (lengths and positions of elements), the equations (14), (15), (17) and (18) lead to:

$$c_1 + c_2 = c_3 + c_4 \; and \; \delta_{aj} = \delta_{ai} \tag{19}$$

The internal forces in Table 2 of a three bars system ($g = 3$) with the barycentric coordinates $c_1 = c_4 = 0.1$ and $c_2 = c_3 = 0.5$, give the self-stable structures in Figure 4 where the constants result from equations (9), (14), (15), (17) and (18).

Table 2. Value of force density in different members

Components	Type of structure	
	Prismatic	Innovative
Horizontal cables δ_h	$-\delta_b$	–
Vertical cables δ_v	$0.5774\delta_h$	–
Struts δ_b	$-\delta_h$	$-1.20\delta_{ai}$
Right cables δ_{rj}	–	$0.25\delta_{ai}$
Right cables δ_{ri}	–	$1.25\delta_{ai}$
Left cables δ_{lj}	–	$1.25\delta_{ai}$
Left cables δ_{li}	–	$0.25\delta_{ai}$
Additional cables $\delta_{ai} = \delta_{aj}$	–	δ_{ai}

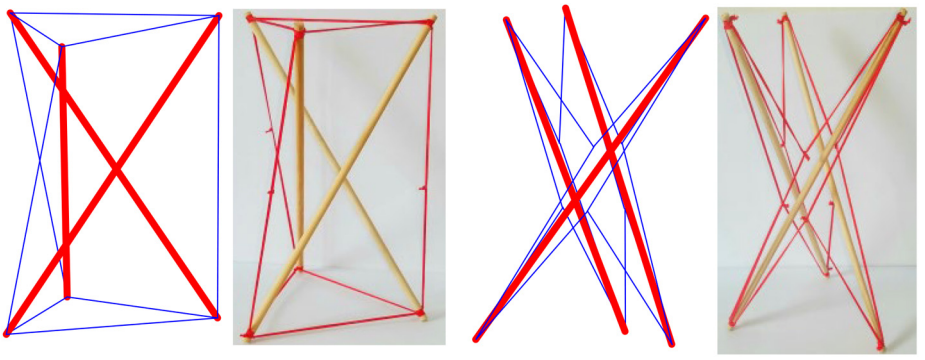

Figure 4.
The closed pattern of three struts tensegrity system

Notes: (a) Prismatic simulation; (b) prismatic real model; (c) novel simulation; (d) novel real model

4.2 Self-stress of class two tensegrity towers

The class of a tensegrity is related to the number of struts meeting at a node. The class-two tensegrity refers to a structure that has two struts meeting at a node. The method for obtaining a class-two tower is connecting "*u*" units by transferring the height h of units linearly and rotating the bottom prism the angle α. The connection of the unitary cells might use a regular shape, same material and size.

The observations made in Masic and Skelton (2005) for tensegrity towers are: the unitary properties remain valid even in the case of loaded towers; in which case, the solutions found in the previous section can be used to characterize the equilibrium configuration and the force densities in all members of the tower structure. Therefore, the overall structure is always stable when the unitary structure is stable.

5. Mass design of tensegrity structures

Being ρ the mass density and A_k and A_w the cross-section areas of the k-th strut and the w-th cable, the mass of struts and cables is:

$$m_k = \rho A_k ||\mathrm{b}_k||;\ m_w = \rho A_w ||\mathrm{s}_w|| \tag{20}$$

From equation (20), the minimal mass can be reached by designing the cross-section area of components according to the constraint of failure. The failure of the structure occurs in two ways: the material may fail (material yields, both struts and cables) or the structure may buckle (material bends: struts). Consequently, the critical cross-section areas for a given uniaxial stress σ of strut and cable subjected to yielding constraint are:

$$A_{ky} \geq \frac{\delta_{bk}||\mathbf{b}_k||}{\sigma} \text{ and } A_{wy} \geq \frac{\delta_{sw}||\mathbf{s}_w||}{\sigma} \tag{21}$$

According to the Euler buckling formula (De Oliveira *et al.*, 2008), a strut of length $||\mathbf{b}_k||$, force density δ_{bk} and young modulus E, under a compressive force $f_b = \delta_{bk}||\mathbf{b}_k||$ buckles if:

$$\delta_{bk}||\mathrm{b}_k|| = \frac{E\pi^3 r_k^4}{4||\mathrm{b}_k||^2} \tag{22}$$

in which r_k is the radius of the strut. From equation (22), it is deduced a cross-section area ensuring the strut does not buckle as:

$$A_{kb} \geq 2||\mathrm{b}_k||\sqrt{\frac{\delta_{bk}||\mathrm{b}_k||}{E\pi}} \tag{23}$$

Thus, by substituting the section areas in equation (20) with those of equation (21) and equation (23), the masses m_{ky} and m_{kb} of a single strut in yielding and buckling failure modes are:

$$m_{ky} := \rho\frac{\delta_{bk}||\mathrm{b}_k||^2}{\sigma};\ m_{kb} := 2||\mathrm{b}_k||^2\rho\sqrt{\frac{\delta_{bk}||\mathrm{b}_k||}{E\pi}} \text{ and } m_{wy} := \rho\frac{\delta_{sw}||\mathrm{s}_w||^2}{\sigma} \tag{24}$$

for a cable in yielding constraint.

The mass of the overall structure having the same material is the sum of the components' mass given as:

$$m_y = \frac{\rho}{\sigma}\left(T_{ky} + T_{wy}\right) \textit{ with } T_{ky} = \sum_k \delta_{bk}||\mathrm{b}_k||^2 \qquad T_{wy} = \sum_w \delta_{sw}||\mathrm{s}_w||^2 \tag{25}$$

for yielding constraint and for buckling constraints

$$m_b = \rho\left(\frac{2T_{kb}}{\sqrt{\pi}} + \sigma^{-1}T_{wy}\right) \textit{ with } T_{kb} = \sum_k \sqrt{\delta_{bk}||\mathrm{b}_k||^5} \tag{26}$$

The next sub-section determines the force of members of loaded structures in Figure 6 to evaluate the mass; this consists of finding the prestress in the components under a defined condition. For this, the tensegrities treated in this paper are compressed with a vertical force f evenly distributed on different top and bottom nodes of struts $f_z = f/g$.

5.1 Mass of a unitary tensegrity structure subjected to a compressive force

The internal forces of struts in Table 2 are negative and appear in equations (25) and (26). Therefore, for a more realistic analysis of the mass, it is considered that all force densities are positive, and the system is subject to the same configuration in both loaded and unloaded conditions. For persevering the twist angle between the bottom and top polygons consistent with equation (2), the proposed algorithm in De Oliveira and Skelton (2009, p. 108); Skelton and De Oliveira (2010) uses a small displacement of vertical cables. With a vertical force f_z on the top node of a strut, the related force in a member that counteracts the applied force produced by the displacement of cables must equal zero. The distribution of forces in different members as represented in Figure 6 are given as

$$\begin{cases} f_z - h_1\delta_v = 0 & \textit{system of Fig. 6(a)} \\ f_z - (1-c_1-c_2)h_1(\delta_{ai} + \delta_{lj} + \delta_{rj}) = 0 & \textit{system of Fig. 6(b)} \\ f_z - (1-c_3-c_4)h_1(\delta_{aj} + \delta_{li} + \delta_{ri}) = 0 & \end{cases} \tag{27}$$

From the relationship between prestresses in the self-balanced system (Table 2) and equation (27), the internal forces in members of the structure subjected to a compressive force are:

$$\delta_v = \delta_b = \frac{f_z}{h_1} \text{ and } \delta_h = 0.5774\frac{f_z}{h_1} \tag{28}$$

$$\begin{pmatrix} \delta_{lj} \\ \delta_{rj} \end{pmatrix} = \begin{pmatrix} \delta_{rj} \\ \delta_{li} \end{pmatrix} = \begin{pmatrix} 1.25{h_1}^{-1}f_z \\ 0.25{h_1}^{-1}f_z \end{pmatrix} \text{ and } \delta_b = 1.2{h_1}^{-1}f_z \tag{29}$$

Introducing equations (26) and (27) into equations (23) and (24), the mass of tensegrities is:

$$\begin{cases} {m_y}^{prsc} = \dfrac{\rho}{\sigma}\left(T_{ky} + {T_{wy}}^{prsc}\right) \; ; \; {m_b}^{prsc} = \rho\left(2\sqrt{\dfrac{1}{\pi E}}T_{kb} + \sigma^{-1}{T_{wy}}^{prsc}\right) \\ {m_y}^{innv} = \dfrac{\rho}{\sigma}\left(1.2T_{ky} + {T_{wy}}^{innv}\right) \; ; \; {m_b}^{innv} = \rho\left(2\sqrt{\dfrac{1.2}{\pi E}}T_{kb} + \sigma^{-1}{T_{wy}}^{innv}\right) \end{cases} \tag{30}$$

in which the superscript "*prsc*" and "*innv*" denote the prismatic and innovative structures respectively. While, due to the configuration, it is implied that the struts of both structures have the same constants T_{ky} and T_{kb} given as:

$$\begin{cases} T_{ky} = f{h_1}^{-1}||\mathbf{b}_k||^2 \\ T_{kb} = \sqrt{f{h_1}^{-1}||\mathrm{b}_k||^5} \end{cases} \tag{31}$$

and the constants ${T_{wy}}^{prsc}$ and ${T_{wy}}^{innov}$ are

$$\begin{cases} {T_{wy}}^{prsc} = {c_s}^{prsc}\dfrac{f}{h_1}; \;\; {c_s}^{prsc} = \; ||\mathrm{s}_v||^2 + 2 \times 0.5774||\mathrm{s}_h||^2 \\ {T_{wy}}^{innov} = {c_s}^{innv}\dfrac{f}{h_1}; \; {c_s}^{innv} = 1.25\left(||\mathbf{s}_{lj}||^2 + ||\mathbf{s}_{ri}||^2\right) + 0.25\left(||\mathbf{s}_{rj}||^2 + ||\mathbf{s}_{li}||^2\right) + ||\mathbf{s}_{ai}||^2 + ||\mathbf{s}_{aj}||^2 \end{cases} \tag{32}$$

5.2 Mass of compressed class two tensegrity structures

Consider now the class two towers in Figure 5 subject to a total compressive load f. The overall height of the structure is h_u, where it is deduced the length of each unit as $h_1 = h_u/u$. In a class two tensegrity structure based on a regular unitary cell, the observation is that f is the vertical load applied to the tower, then f is the vertical force evenly applied at each unit. Therefore, the total mass of struts and cables is:

$$\begin{cases} {M_y}^{prsc} = \dfrac{\rho}{u\sigma}\left(T_{ky} + {T_{wy}}^{prsc}\right) \; ; \; {M_b}^{prsc} = \dfrac{\rho}{u\sqrt{u}}\left(2u\sqrt{\dfrac{1}{\pi E}}T_{kb} + \dfrac{\sqrt{u}}{\sigma}{T_{wy}}^{prsc}\right) \\ {M_y}^{innv} = \dfrac{\rho}{u\sigma}\left(1.2T_{ky} + {T_{wy}}^{innv}\right) \; ; \; {M_b}^{innv} = \dfrac{\rho}{u\sqrt{u}}\left(2u\sqrt{\dfrac{1.2}{\pi E}}T_{kb} + \dfrac{\sqrt{u}}{\sigma}{T_{wy}}^{innv}\right) \end{cases} \tag{33}$$

6. Analysis: mass ratio and structural comparison

Let us mention that this analysis does not concern the structures subject to yielding constraints due to the following fact: the mass ratio is a function of the geometric parameters

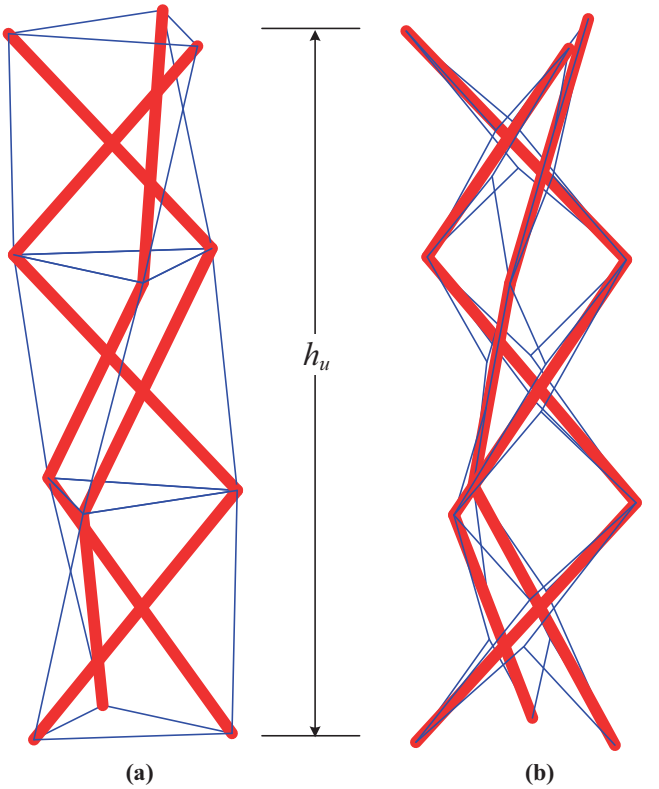

Figure 5.
Tensegrity class-two towers made by stacking three unitary cells

Notes: (a) Prismatic class two tensegrity tower; (b) innovative class two tensegrity tower

and does not offer an overall prospect on the variation of applied forces. As an illustration, the mass ratio of a prism tensegrity subjected to yielding constraints is:

$$\eta_y^{prsm} = \frac{||\mathbf{b}_k||^2 + c_s^{prsc}}{gu^2 h_1^2} \tag{34}$$

6.1 Mass ratio

From the equations of minimal mass in Section 5, the mass ratio is given as the mass of a tensegrity system versus the mass of a single element ($m_1 = 2\rho h_u^2 (f/\pi E)^{1/2}$: strut subject to buckling constraint), both having the same width ($2r$) and length (h_u). In particular, once the consideration is the buckling constraint, the evaluation of the mass ratio is made possible by:

$$\eta_b^{prsc} = \sqrt{3} c_b + \chi \frac{0.5 c_s^{prsc}}{(h_1 u)^3} \quad ; \quad c_b = \frac{\sqrt{||\mathbf{b}_k||^5 (h_1 u)^{-1}}}{(h_1 u)^2} \quad \chi = \sqrt{\frac{f\pi}{\sigma^2}} \tag{35}$$

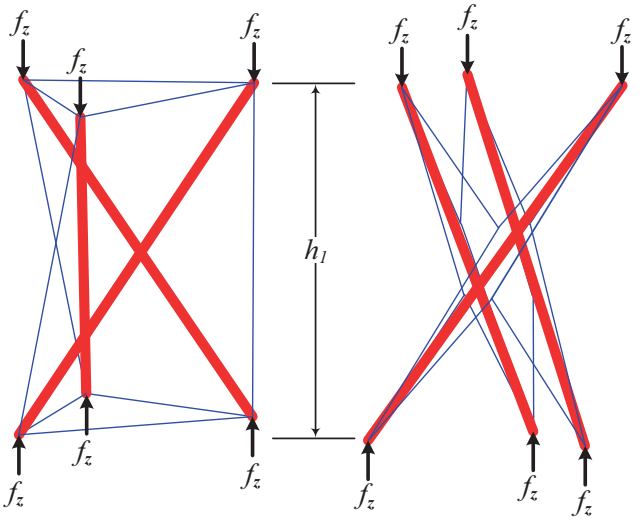

(a) **(b)**

Notes: (a) Three struts prismatic tensegrity under a compressive force f; (b) a compressed three struts innovative tensegrity by a force f. The height of the structure is noted as h_1 instead of h

Figure 6. Tensegrity system loaded with a vertical force f

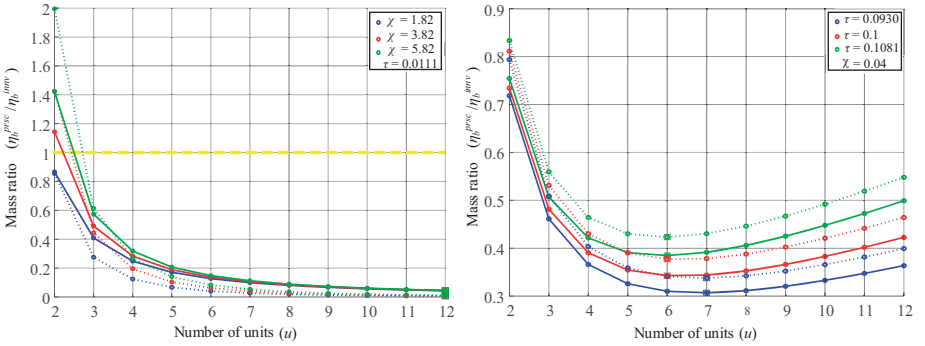

(a) **(b)**

Notes: (a) Simulated mass ratio considering the variable τ fixed; (b) mass ratio of prismatic and innovative tensegrity with variable χ fixed. The dotted lines represent the regressive curve of η_b^{innv}, and the continuous lines represent η_b^{prsc}

Figure 7. Comparative graphs of mass ratio versus the number of stages

$$\eta_b^{innv} = \sqrt{3.6}c_b + \chi\frac{0.5c_s^{innv}}{(h_1 u)^3} \tag{36}$$

leading to anticipate that at a certain number of units, both tensegrities reduce their mass via the number of struts and cells, which can be perceived in Figure 7.

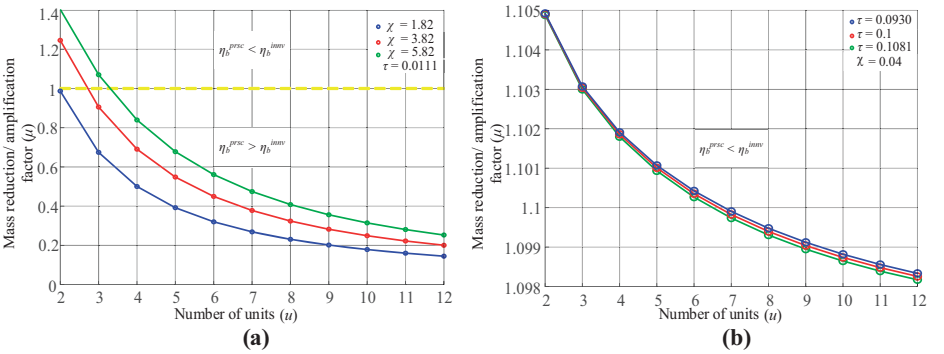

Figure 8.
The regressive curve of the mass reduction/ amplification factor

Notes: (a) Simulated mass ratio considering the variable τ fixed; (b) mass ratio of prismatic and innovative tensegrity with variable χ fixed

The first analysis condition illustrated by setting the radius ratio and the height of a unitary cell as a constant ($\tau = r/h_1$) and varying χ demonstrates the mass of both structures reaches the minimum value when the number of units increases [Figure 7(a)]. However, it is observed that, under a defined load condition, the proposed model outperforms the triangular prismatic tensegrity. The next sub-section overcomes this by a structural comparison with a *mass reduction/amplification factor* for determining the best performance in terms of reduction of mass between the two systems.

Although the constants χ and r are fixed, the variation of the total height h_u to obtain the ratio $\tau = r/h_u$ shows that the mass of tensegrities decreases till the minimum value (marked with square symbols) and afterward increases with the number of stages [Figure 7(b)]. The minimum mass of $\tau = \{0.0930, 0.1, 0.1081\}$ is reached for the number of units equal to $u = \{6, 6, 7\}$; in this perspective, the number of iterations which gives the minimal mass value increases with the geometric parameters τ.

Furthermore, the regressive curves of mass ratio show that mass linearly decreases with τ and in the opposite decreases with the linear increment of χ. For instance, in Figure 7(b), the radius of the structure can be fixed and adjust the total height to meet the desired design.

6.2 Structural comparison

Even though both structures seem to outperform a single element, there is still doubt about their mass saving performance. For this, it is introduced a mass reduction/amplification factor as the ratio between $\eta_b{}^{innv}$ and $\eta_b{}^{prsc}$ calculated as:

$$\mu = \frac{\eta_b{}^{innv}}{\eta_b{}^{prsc}} \tag{37}$$

The reliability of the new tensegrity system as a mass saving structure can be illustrated with $\mu < 1$; in the opposite, it becomes an amplification factor.

The gap between the masses of the structures is more visible for the factor μ when the variable τ is fixed compared to the gap of the nonlinear regressive curve μ when the variable χ is fixed and this explains the foremost influence factor between χ and τ. It is observed through Figure 8(a) that the curves converge to the same value, and in Figure 8(b), the curves diverge after a fourth stage.

The innovative tensegrity plays a mass amplification role for $\chi = \{3.82, 5.82\}$ by where $u < \{3, 4\}$ [Figure 8(a)] and keeps the same properties in circumstances of χ constant and τ variable.

7. Conclusions

This paper aimed to analyze the influence of the geometry and external forces on the minimal mass design of two tensegrity systems. The methodology used in this work yields in the determination of prestress distribution and parameterizes the mass in buckling failure mode under a compressive force. The analysis conducted, when the consideration is the geometry, shows that the mass ratio decreases with an increase of stages and afterward increases after the minimum mass is reached. In the view of external force, it is seen that when the cells increase the most, the structure's mass decreases compared to a single element. In the same mode of failure (buckling mode), one can use the proposed model to save mass if the variation considers the external forces. On the other hand, the prismatic tensegrity is reliable as a mass saving structure when the mechanical properties of materials and forces ensure that χ is less than or equal to 0.04.

References

Agogino, A. Sunspiral, V. and Atkinson, D. (2013), "Super ball bot-structures for planetary landing and exploration for the NASA innovative advanced concepts (NIAC) program NASA innovative advanced concepts",

Amendola, A., Carpentieri, G., de Oliveira, M., Skelton, R.E. and Fraternali, F. (2014), "Experimental investigation of the softening-stiffening response of tensegrity prisms under compressive loading", *Composite Structures*, Vol. 117 No. 1, pp. 234-243.

Averseng, J. and Dubé, J.F. (2012), "Design, analysis and self stress setting of a lightweight deployable tensegrity modular structure", *Procedia Engineering*, Vol. 40, pp. 14-19.

Caluwaerts, K., Bruce, J., Friesen, J.M. and Sunspiral, V. (2016), "State estimation for tensegrity robots", *Proceedings – IEEE International Conference on Robotics and Automation, Vol. 2016, IEEE*, pp. 1860-1865.

Chen, M. and Skelton, R.E. (2020), "A general approach to minimal mass tensegrity", *Composite Structures, Vol. 248*, Elsevier Ltd, p. 112454.

Chen, Y., Feng, J., Lv, H. and Sun, Q. (2018), "Symmetry representations and elastic redundancy for members of tensegrity structures", *Composite Structures*, Vol. 203, pp. 672-680.

Chen, Y., Yan, J., Sareh, P. and Feng, J. (2020), "Feasible prestress modes for cable-srut structures with multiple self-stress states using particle swarm optimization", *Journal of Computing in Civil Engineering*, Vol. 34 No. 3, pp. 1-10.

De Oliveira, M.C. and Skelton, R.E. (2009), *Tensegrity Systems, Vol. 1*, Springer, Dordrecht, Heidelberg, London, New York, NY, available at: https://doi.org/10.1007/978-0-387-74242-7

De Oliveira, M.C., Skelton, R.E. and Chan, W. (2008), "Minimum mass design of tensegrity towers and plates", *Proceedings of the 45th IEEE Conference on Decision and Control, IEEE*, pp. 2314-2319.

Fazli, N. and Abedian, A. (2011), "Design of tensegrity structures for supporting deployable mesh antennas", *Scientia Iranica*, Vol. 18 No. 5, pp. 1078-1087.

Fraddosio, A., Pavone, G. and Piccioni, M.D. (2019), "Minimal mass and self-stress analysis for innovative V-Expander tensegrity cells", *Composite Structures*, Vol. 209, pp. 754-774.

Fraternali, F., Senatore, L. and Daraio, C. (2012), "Solitary waves on tensegrity lattices", *Journal of the Mechanics and Physics of Solids*, Vol. 60 No. 6, pp. 1137-1144.

González, A., Luo, A. and Liu, H. (2017), "Study of a novel design for self-standing tensegrity domes", *International Association for Shell and Spatial Structures*, Vol. 1, pp. 1-8.

Goyal, R., Peraza Hernandez, E.A. and Skelton, R.E. (2019), "Analytical study of tensegrity lattices for mass-efficient mechanical energy absorption", *International Journal of Space Structures*, Vol. 34 Nos 1/2, pp. 3-21.

Goyal, R., Skelton, R.E. and Peraza Hernandez, E.A. (2020), "Design of minimal mass load-bearing tensegrity lattices", *Mechanics Research Communications*, Vol. 103, available at: https://doi.org/10.1016/j.mechrescom.2020.103477

Iscen, A., Agogino, A., SunSpiral, V. and Tumer, K. (2013), "Controlling tensegrity robots through evolution", in Blum, C. (Ed.), *Proceeding of the 15th Annual Conference on Genetic and Evolution Computation*, Association for Computing Machinery, New York, NY, pp. 1293-1300.

Kawaguchi, K. and Lu, Z.-Y. (2002), "Construction of three-strut tension systems", in Parke, G. and Disney, P. (Eds), *Proceeding of the Fifth International Conference on Space Structures*, pp. 1-10.

Kim, K., Agogino, A.K. and Agogino, A.M. (2020), "Rolling locomotion of cable-driven soft spherical tensegrity robots", *Soft Robotics*, Vol. 7 No. 3, pp. 1-16.

Koohestani, K. (2017), "On the analytical form-finding of tensegrities", *Composite Structures*, Vol. 166, pp. 114-119.

Koohestani, K. and Guest, S.D. (2013), "A new approach to the analytical and numerical form-finding of tensegrity structures", *International Journal of Solids and Structures*, Vol. 50 No. 19, pp. 2995-3007. Elsevier Ltd,

Liu, H., Geng, J. and Luo, A. (2017), "Tensegrity configuration method for connecting tensegrity units along their axes", *Composite Structures*, Vol. 162, pp. 341-350.

Liu, H., Zhang, J. and Ohsaki, M. (2018), "New 3-bar prismatic tensegrity units", *Composite Structures*, Vol. 184, pp. 306-313.

Luo, A., Heping, L., Skelton, R.E. and Shijun, C. (2018), "The theory of basic tensegrity unit stable forming", *Journal of Mechanical Engineering*, Vol. 53 No. 23, pp. 62.

Ma, S., Yuan, X. and Samy, A. (2019), "Shape optimization of a new tensegrity torus", *Mechanics Research Communications*, Vol. 100, p. 103396.

Masic, M. and Skelton, R.E. (2005), "Path planning and open-loop shape control of modular tensegrity structures", *Journal of Guidance, Control, and Dynamics*, Vol. 28 No. 3, pp. 421-430.

René Motro (2003), *Tensegrity: Structural Systems for the Future*, Butterworth-Heinemann, available at: https://doi.org/10.1016/B978-190399637-9/50033-0

Skelton, R.E. and De Oliveira, M.C. (2010), "Optimal complexity of deployable compressive structures", *Journal of the Franklin Institute*, Vol. 347 No. 1, pp. 228-256.

Skelton, R.E., Montuori, R. and Pecoraro, V. (2016), "Globally stable minimal mass compressive tensegrity structures", *Composite Structures*, Vol. 141, pp. 346-354.

Sultan, C., Corless, M. and Skelton, R.E. (2002), "Symmetrical reconfiguration of tensegrity structures", *International Journal of Solids and Structures*, Vol. 39 No. 8, pp. 2215-2234.

Tibert, A.G. and Pellegrino, S. (2003), "Review of form-finding methods for tensegrity structures", *International Journal of Space Structures*, Vol. 18 No. 4, pp. 209-223.

Tran, H.C. and Lee, J. (2010), "Advanced form-finding of tensegrity structures", *Computers and Structures*, Vol. 88 No. 3-4, pp. 237-246. No. 3–4,

Vumiliya, A., Luo, A. and Song, Z. (2018), "Mathematic modeling for configuration of tensegrity structure", *2018 IEEE International Conference on Mechatronics and Automation (ICMA), IEEE*, pp. 104-109.

Xu, X. and Luo, Y. (2010), "Form-finding of nonregular tensegrities using a genetic algorithm", *Mechanics Research Communications*, Vol. 37 No. 1, pp. 85-91.

Zhang, J.Y., Guest, S.D., Connelly, R. and Ohsaki, M. (2010), "Dihedral 'star' tensegrity structures", *International Journal of Solids and Structures*, Vol. 47 No. 1, pp. 1-9.

Zhang, L.Y., Zhu, S.X., Li, S.X. and Xu, G.K. (2018), "Analytical form-finding of tensegrities using determinant of force-density matrix", *Composite Structures*, Vol. 189, pp. 87-98.

Zolesi, V.S., Donati, A., Ghiozzi, M., Ganga, P.L., Podio-Guidugli, P., Scolamiero, L., Micheletti, A., et al. (2013),. "On an innovative deployment concept for large space structures", *42nd International Conference on Environmental Systems, San Diego*, pp. 1-14.

Corresponding author
Angelo Vumiliya can be contacted at: vuange@gmail.com